

Intrinsic kinetics of propane hydrate formation

Sebastien Bergeron and Phillip Servio*

Department of Chemical Engineering, McGill University, Canada

Abstract

A considerable amount of research is being conducted on gas hydrates due to their potential applications, including naturally occurring methane hydrates as an alternate energy source, carbon dioxide sequestration as a means to mitigate the global warming effect, and storage and transportation of natural gas hydrates over more traditional methods such as liquefied natural (LNG) gas or compressed natural gas (CNG). Hence, large scale production of gas hydrates represents a promising new technology, which requires in-depth understanding of hydrate kinetics, including the intrinsic reaction rate constant for proper reactor design. Consequently, experimental data on the rate of formation of propane hydrates was obtained using a particle size analyzer capable of detecting particles with diameters as small as 0.6 nanometers, while operating in a closed loop system. Experiments were carried out at a temperature of 274 K and pressures between 212 and 261 kPa in a semi-batch stirred tank reactor. The experimental data was analyzed using a newly developed kinetic model based on crystallization theory and as a result, the actual reaction rate constant for propane hydrate formation was successfully determined.

Keywords: gas hydrate, kinetics, reaction rate constant, particle size analysis, crystallization

1. Introduction

Gas hydrates are crystalline solids that form when a gas or a volatile liquid molecule suitable for hydrate formation is enclosed in a network consisting of water molecules linked together through hydrogen bonding. The presence of the hydrate forming gas molecule stabilizes the water lattice through physical bonding via weak van der Waals forces. Up to now, four hydrate structures have been reported, including structure I (sI), structure II (sII) and structure H (sH). Considerable research is being conducted on gas hydrates due to their potential applications, including methane hydrates as an alternate energy source, storage and transportation of natural gas hydrates or liquefied petroleum gases and carbon dioxide sequestration. Such promising new technologies are

* Corresponding author Tel.: +1-514-398-1026 ; fax: +1-514-398-6678
E-mail address: phillip.servio@mcgill.ca

reasons why kinetics studies should be further investigated. Figure 1 below shows the three-phase equilibrium line for the propane-water system using the experimental data of Deaton and Frost [1], where hydrate, liquid water and vapor are at equilibrium (H-L_w-V). Above the three-phase line, hydrate-liquid water is present (H-L_w), while below the line, vapor-liquid water is present (V-L_w).

Various studies have been conducted to determine the reaction rate constant of gas hydrates. Englezos et al. [2, 3] performed experiments using methane and ethane gas hydrates without any particle size distribution measurement. They used an average linear growth based on a population balance and assumed homogeneous nucleation. Malegaonkar et al. [4] repeated the same procedure (no particle size distribution measurement) and assumptions made previously by Englezos et al, but for methane and carbon dioxide gas hydrates. More recently, Clarke and Bishnoi have performed experiments to determine the intrinsic reaction rate constant for various hydrate systems [5-7]. Throughout their work [5, 8, 9], they used ex-situ and in-situ particle size analyzers to obtain the particle size distribution of both carbon dioxide and ethane gas hydrates, as well as mixtures of methane and ethane hydrates. The apparatus used allowed them to measure particles with chord lengths as small as 0.5 μm. Due to instrument limitations, they had to extrapolate their particle size distributions for diameters smaller than 0.5 μm. In addition, their analysis assumed homogeneous nucleation, while their model neglected the interfacial resistance at the vapor-liquid water interface. Recently, Hashemi et al. [10] have highlighted some points that need to be addressed concerning the determination of the intrinsic reaction rate constant of hydrate formation.

The current work proposes a newly developed kinetic model based on the work of Englezos et al. [2], as well as a novel experimental setup to accurately measure the true reaction rate constant for propane hydrates. This work can be readily expanded to other hydrate systems, including methane and carbon dioxide gas hydrates.

2. Experimental apparatus and procedure

2.1 Apparatus

As shown on Figure 2, the current experimental setup consists of an isothermal/isobaric semi-batch stirred tank reactor, a gas supply reservoir for hydrate formation and a *Zetasizer Nano ZS* particle size analyzer (*Malvern*

Instruments). Hydrates are formed in the 600 cm³ internal volume stainless steel reactor (12 000 kPa pressure rating). A *PPI DYNA/MAG MM-006* mixer (0-2500 rpm) has been mounted on top of the reactor to ensure sufficient mixing. Gas is supplied from the stainless steel reservoir (internal volume of 300 cm³) using a *Baumann 51000 Series Low Flow* control valve. Both the reactor and the reservoir are submerged in a cooling bath controlled via a *Thermo NESLAB RTE Series* refrigerated bath. The liquid phase is continuously circulated through a flow cell with a 500 kPa pressure rating (*Hellma*) in the *Zetasizer Nano ZS* particle size analyzer by means of a *LabAlliance Model 1500* dual piston pump. The *Zetasizer Nano ZS* particle size analyzer is capable of detecting particles with diameters ranging from 0.6 nanometers to 6 microns. Temperature and pressure measurements are performed using standard resistance temperature devices and *Rosemount 3051S Series* pressure transducers. The readouts are then recorded and displayed using the *National Instruments NI-DAQ 7* data acquisition device and the *LabVIEW* software. The *LabVIEW* interface was written to calculate the number of moles of gas in the hydrate phase at any time during the experiment using the Trebble-Bishnoi equation of state [11].

2.2 Procedure

Prior to any experiment, the reactor is cleaned using double distilled/de-ionized water and purged several times using the selected gas (instrument grade, 99.5%). A syringe is used to introduce 180 ml of double distilled/de-ionized water and the dual piston pump is started. Once thermal equilibrium has been reached, the reactor is pressurized above the three-phase equilibrium pressure at the experimental temperature (Figure 1). Once the temperature in the reservoir and in the reactor has stabilized, both the data acquisition program and the reactor stirrer are started. Figure 3 below shows a typical mole consumption plot for a kinetic experiment using propane. When the mole consumption deviates from its turbidity value (onset of growth), a particle size distribution measurement is performed in order to determine the critical nuclei diameter. Accordingly, the dual piston pump is shut off and the particle size analyzer is isolated by means of manual valves and a measurement is performed. Once the measurement is completed, the manual valves are reopened and the dual piston pump is restarted. Various particle size distribution measurements are conducted at regular time intervals to properly describe the growth stage of hydrate formation.

3. Theory

3.1 Determination of the reaction rate constant from a new kinetic model

The newly developed kinetic model was derived using crystallization theory and is based on the Englezos model [2, 3]. The overall resistance to hydrate growth is represented by:

$$R = \frac{1}{A_p} \left(\frac{1}{k_{H-L}^l} + \frac{1}{k_r} \right) + \frac{1}{K_{OL}} \quad (1)$$

where A_p is the total solid surface area (hydrate particles), k_{H-L}^l is the mass transfer coefficient in the diffusion layer around the hydrate particle, k_r is the reaction rate constant and $\frac{1}{K_{OL}}$ is the V-L_w interfacial resistance.

From a scaling analysis [12], it follows that the resistance on the gas side of the V-L_w interface is negligible compared to that on the liquid side. Moreover, the *Sherwood* number for solid particles in an agitated vessel is given by [13]:

$$Sh = \frac{k_{H-L}^l L}{D} = 2 + 0.6 Re^{1/2} Sc^{1/3} \quad (2)$$

Assuming a stagnant film, in other words the lowest mass transfer coefficient, and using the correlation of Wilke and Chang [14] with the parameters of Hayduk and Laudie [15] to estimate the diffusion coefficient of the gas hydrate former in water, it follows that the diffusivity, D , is in the order of 10^{-6} - 10^{-7} m²/s and thus, k_{H-L}^l is in the order of 10^{-1} - 10^0 m/s. On the other hand, previous work performed by Clarke and Bishnoi [6] showed that k_r for carbon dioxide hydrates (sI) formation is in the order of 10^{-8} m/s. Therefore, it is reasonable to assume that $\frac{1}{k_{H-L}^l}$ is negligible compared to $\frac{1}{k_r}$.

Using eq. (1) and the driving force proposed in the work of Hashemi et al. [10], the number of moles consumed for hydrate growth is given by:

$$\left(\frac{dn}{dt}\right) = \frac{C_{w0}(x_{L-V}^i - x_{H-L}^i)}{\frac{1}{A_p k_r} + \frac{1}{k_{L-V}^l A_{L-V}}} \quad (3)$$

where C_{w0} is the initial concentration of water in the bulk liquid phase (assumed constant), x_{L-V}^i is the gas hydrate former solubility in the liquid phase at the V-L_w interface under hypothetical V-L_w equilibrium (T_{exp} , P_{exp}) and x_{H-L}^i is the gas hydrate former solubility in the liquid phase at the H-L_w interface under H-L_w equilibrium (T_{exp} , P_{exp}).

Expressing the total solid surface area as a function of the second moment of the particle size distribution, eq. (3) becomes:

$$\left(\frac{dn}{dt}\right) = \frac{C_{w0}(x_{L-V}^i - x_{H-L}^i)}{\frac{1}{\pi\mu_2 V_L k_r} + \frac{1}{k_{L-V}^l A_{L-V}}} \quad (4)$$

where V_L is the volume of liquid in the reactor and the second moment of the particle size distribution is defined as [16]:

$$\mu_2(t) = \int_0^{\infty} L^2 \varphi(L, t) dL \quad (5)$$

where L is the hydrate diameter and φ is the particle density distribution.

Assuming no breakage, no agglomeration and no secondary nucleation, the initial number of particles is given by:

$$\mu_0^0 = \frac{6MW_H(n_{tb} - n_{eq})}{\pi V_L \rho_H L_c^3} \quad (6)$$

where n_{tb} is the number of moles of gas hydrate former dissolved at turbidity, i.e. at the onset of growth, and n_{eq} is the number of moles of gas hydrate former dissolved under H-L_w equilibrium.

The critical nuclei diameter (L_c) is determined by taking the mean diameter from the particle size distribution obtained at the onset of growth, which accounts for both homogeneous and heterogeneous nucleation.

In order to calculate the particle density distribution, the cumulative oversize particle distribution (γ) is first obtained using eq. (6) and the various particle size distributions (obtained experimentally from the *Zetasizer Nano ZS*) by fitting a log normal function. Then, the particle density distribution is calculated as follow:

$$\varphi = \frac{d\gamma}{dL} \quad (7)$$

after which the second moment is calculated using both eq. (5) and eq. (7).

Rearranging eq. (4), the reaction rate constant can be determined:

$$\left(\frac{dn}{dt}\right) = \frac{V_L \rho_w}{MW_w} * \frac{(x_{L-V}^i - x_{H-L}^i)}{\frac{1}{\pi \mu_2 k_r} + \frac{1}{k_{L-V}^l a_{L-V}}} \quad (8)$$

where ρ_w is the density of water at T_{exp} , MW_w is the molecular weight of water and $k_{L-V}^l a_{L-V}$ is the dissolution rate in the film at the V-L_w interface.

3.2 Determination of the reaction rate constant using a population balance

The reaction rate constant can also be derived from a semi-theoretical approach using the newly developed kinetic model and a population balance. In particular, assuming that there is no breakage or agglomeration, the population balance for a batch crystallizer yields [16]:

$$\frac{d\varphi}{dt} + \frac{d(G\varphi)}{dL} = 0 \quad (9)$$

where G is the growth rate.

Using the mean diameter obtained for each particle size distribution measurement performed, an expression for the growth rate can be obtained using the following:

$$G = \frac{dL}{dt} \quad (10)$$

Eq. (9) can then be transformed into a set of differential equations and performing the moment transformations [16]:

$$\frac{d\mu_j}{dt} = jG\mu_{j-1} \quad (11)$$

Hence, solving eq. (11):

$$\mu_0 = \mu_0^0 \quad (12)$$

$$\mu_1 = \mu_0^0 Gt + \mu_1^0 \quad (13)$$

$$\mu_2 = \mu_0^0 G^2 t^2 + 2\mu_1^0 Gt + \mu_2^0 \quad (14)$$

where μ_0 , μ_1 and μ_2 are the zeroth, first and second moment respectively.

Incorporating equation (14) into equation (4):

$$\left(\frac{dn}{dt}\right) = \frac{C_{W0}(x_{L-V}^i - x_{H-L}^i)}{\frac{1}{\pi(\mu_0^0 G^2 t^2 + 2\mu_1^0 Gt + \mu_2^0)} V_L k_r} + \frac{1}{k_{L-V}^l A_{L-V}} \quad (15)$$

The initial number of particles (μ_0^0) is given by equation (6), while μ_1^0 and μ_2^0 are given by:

$$\mu_1^0 = L_c \mu_o^0 \quad (16)$$

$$\mu_2^0 = L_c^2 \mu_o^0 \quad (17)$$

It follows that eq. (15) can be rewritten as:

$$\left(\frac{dn}{dt}\right) = \frac{V_L C_{W0}(x_{L-V}^i - x_{H-L}^i)}{\frac{1}{\pi(\mu_0^0 G^2 t^2 + 2L_c \mu_o^0 Gt + L_c^2 \mu_o^0)} k_r} + \frac{1}{k_{L-V}^l a_{L-V}} \quad (18)$$

from which the reaction rate constant can be determined.

3.3 Determination of the dissolution rate in the film at the vapor-liquid water interface

Solubility experiments were conducted to determine the dissolution rate in the film at the V-L_w interface, as required in eq. (8) and eq. (18). Neglecting the resistance on the gas side of the V-L_w interface (section 3.1) and

assuming that the total number of moles is constant and equal to the initial number of moles of water in the liquid phase, the rate at which gas is dissolving can be expressed as:

$$\left(\frac{dx}{dt}\right) = k_{L-V}^l a_{L-V} (x_{L-V}^i - x) \quad (19)$$

4. Results and discussion

Solubility experiments were first performed to determine the dissolution rate in the film at the vapor-liquid water interface. These experiments were performed at the same temperature as the kinetic experiments, but at slightly lower pressures to ensure that the system was under V-L_w equilibrium. The reactor stirrer was also set to the same speed as for the kinetic experiments, i.e. 750 rpm. All variables contained in eq. (19) were obtained experimentally from the solubility experiments, except for the dissolution rate which was calculated using a least square analysis. Experiments conducted at 274.2 K and 150.0 kPa yielded a dissolution rate of 2.15E-3 s⁻¹ with an average absolute relative error of 4.1 %.

Kinetic experiments were performed to determine the reaction rate constant for propane hydrate (sII) formation. Experiments were conducted at 274 K and pressures between 212 and 261 kPa. When calculating the initial number of particles, it is assumed that it remains constant throughout the entire experiment and thus, that secondary nucleation, breakage and agglomeration are negligible. To foster such a hypothesis, the mean count rate, which is an indication of the number of photons detected per second, was monitored on a continuous basis using the *Zetasizer Nano ZS*. Since the current setup analyses only a very small sample of the liquid phase, it is expected that the mean count rate will fluctuate through time. Nevertheless, a relatively constant mean count rate (order of magnitude) implies that the number of particles remains constant, while a steadily increasing or decreasing count rate indicates an aggregating or sedimenting sample respectively. As seen on Figure 4, the order of magnitude of the mean count remains relatively constant throughout the experiment, even before and after the onset of growth, which validates the assumptions made when calculating the number of particles. Furthermore, particle size distribution measurements performed at the onset of growth revealed a mean diameter of 113 nm at 274.1 K and 261.0 kPa. Such a critical nuclei diameter is well above the reported value

for homogeneous nucleation [2] and when combined with the relatively constant count rate, it is reasonable to assume that nucleation was primarily heterogeneous. In addition, the value obtained for the critical nuclei diameter will vary from one experiment to the other depending on the size of the impurities (acting as nucleation sites) found in the solution.

To calculate the reaction rate constant using eq. (8), an expression for the mole consumption rate after the onset of growth was obtained from the experimental mole consumption plot. Due to a lack of available models for the propane-water system, x_{L-V}^i was calculated using the fugacity of pure propane in the vapor phase at the experimental temperature and pressure, based on the Trebble-Bishnoi equation of state [11], as well as using a hypothetical Henry's constant ($T_{\text{exp}}, P_{\text{exp}}$) from the correlation of Chapoy et al. [17]. As for x_{H-L}^i , it was obtained from the solubility experiments of Gaudette et al [18]. The second moment, which follows a second order behavior, was obtained experimentally (section 3.1) and is displayed in Figure 5.

The reaction rate constant was then determined using eq. (8) and a least square analysis. Using the dissolution rate obtained experimentally ($2.15\text{E-}3 \text{ s}^{-1}$) yielded a reaction rate constant that could vary from 10 orders of magnitude without having a significant impact. It was evident that the value obtained from the solubility experiments was underestimated and thus, the resistance at the vapor-liquid water interface was overestimated. The dissolution rate is a function of temperature, geometry and rheology. Consequently, the presence of hydrate crystals could modify the interfacial area at the vapor-liquid water interface, while altering the viscosity of the bulk solution. Since the mass transfer coefficient at the vapor-liquid water interface scales with the diffusion coefficient of the gas hydrate former, a change in the bulk viscosity will impact the mass transfer coefficient. Hence, both the reaction rate constant and the dissolution rate were determined using eq. (8) and a least square analysis. It is believed that initially, the resistance to hydrate growth will be mostly due to kinetics, the bulk solution being supersaturated. However, as the hydrate particles grow, the solution becomes depleted in gas and accordingly, the resistance due to mass transfer gradually increases. Using an iterative procedure, both the reaction rate constant and the dissolution rate were optimized simultaneously, the former over the parabolic portion of the mole consumption plot, the latter over the linear portion. Using such an approach, the kinetic experiments yielded a reaction rate constant of $1.48\text{E-}5 \text{ m/s}$ and a dissolution rate of $1.73\text{E-}2 \text{ s}^{-1}$ at 274.1 K .

Figure 6 shows the comparison between the mole consumption rate obtained experimentally and the kinetic model, with an average absolute relative error of 4.5 %. The ratio of the kinetic resistance to the mass transfer resistance at the vapor-liquid water interface was also included. It can be seen that the importance of the kinetic resistance gradually decreases as time progresses, the system becoming more and more mass transfer limited.

Due to inaccurate hydrate surface area measurements [10], researchers have not been able so far to relate the reaction rate constant obtained experimentally to the one obtained from a population balance. Consequently, the reaction rate constant was also calculated using eq. (18) and compared to the value obtained using eq. (8). The same procedure was used as in the case of eq. (8), except for the second moment which was calculated using a population balance and an average linear growth rate (section 3.2). Again, both the reaction rate constant and the dissolution rate were obtained using a least square analysis. Figure 7 shows a similar trend as that obtained in Figure 6, with a reaction rate constant of $8.20\text{E-}6$ m/s and a dissolution rate of $1.76\text{E-}2$ s⁻¹ at 274.1 K.

Moreover, the AARE between the model and the experimental mole consumption rate is 3.1 %. The discrepancy between the reaction rate constant obtained experimentally and that from a population balance is due to the assumption of a linear growth rate in the latter case. Indeed, the second moment obtained from the population balance is constantly well above that measured experimentally. According to eq. (8) and for a given kinetic resistance, the reaction rate constant will decrease when the second moment increases, explaining the smaller reaction rate constant obtained from the population balance.

5. Conclusion

The reaction rate constant for propane hydrate (sII) formation was successfully determined ($1.48\text{E-}5$ m/s at 274.1 K) using a novel experimental setup and a newly developed kinetic model. The particle size analyzer used in the current work could detect particles from 0.6 nanometers to 6 microns in diameter, which is well within the range of particle sizes involved in hydrate growth, including the critical nuclei diameter.

Acknowledgements

The authors are grateful to the Natural Sciences and Engineering Research Council of Canada for financial assistance, as well as the Canada Research Chair program and the Canadian Foundation for Innovation.

List of symbols

a	vapor-liquid interfacial area per unit volume of dispersion (m^{-1})
A_{L-V}	vapor-liquid interfacial area (m^2)
A_p	total solid surface area (m^2)
D	binary diffusion coefficient ($\frac{m^2}{s}$)
G	growth rate ($\frac{m}{s}$)
k	mass transfer coefficient ($\frac{m}{s}$)
$\frac{1}{K_{OL}}$	vapor-liquid interfacial resistance ($\frac{s}{m^3}$)
k_r	reaction rate constant ($\frac{m}{s}$)
L	hydrate diameter (m)
L_c	critical hydrate diameter (m)
MW	molecular weight ($\frac{g}{mol}$)
n	moles
R	resistance ($\frac{s}{m^3}$)
Re	Reynolds number
Sc	Schmidt number
Sh	Sherwood number
t	time (s)

μ_0	zeroth moment of the particle size distribution (m^{-3})
μ_1	first moment of the particle size distribution (m^{-2})
μ_2	second moment of the particle size distribution (m^{-1})
V_L	volume of liquid (m^3)
x	mole fraction
ρ	density $\left(\frac{g}{m^3}\right)$
π	Pi
ϕ	particle density distribution $\left(\frac{particles}{m^4}\right)$
γ	cumulative oversize particle distribution $\left(\frac{particles}{m^3}\right)$

Subscripts

eq	equilibrium
H	hydrate
$H - L$	hydrate-liquid water
$L - V$	vapor-liquid water
tb	turbidity
w	water

Superscripts

i	interface
-----	-----------

References

- [1] E.D. Sloan, Clathrate Hydrates of Natural Gases, Marcel Dekker Inc., New York, 1998.

- [2] P. Englezos, N. Kalogerakis, P.D. Dholabhai, P.R. Bishnoi, *Chemical Engineering Science*. 42 (1987) 2647-2658.
- [3] P. Englezos, N. Kalogerakis, P.D. Dholabhai, P.R. Bishnoi, *Chemical Engineering Science*. 42 (1987) 2659-2666.
- [4] M.B. Malegaonkar, P.D. Dholabhai, P.R. Bishnoi, *The Canadian Journal of Chemical Engineering*. 75 (1997) 1090-1099.
- [5] M. Clarke, P.R. Bishnoi, *Chemical Engineering Science*. 55 (2000) 4869-4883.
- [6] M. Clarke, P.R. Bishnoi, *Chemical Engineering Science*. 60 (2005) 695-709.
- [7] M. Clarke, P.R. Bishnoi, *The Canadian Journal of Chemical Engineering*. 79 (2001) 143-147.
- [8] M. Clarke, P.R. Bishnoi, *Chemical Engineering Science*. 59 (2004) 2983-2993.
- [9] M. Clarke, P.R. Bishnoi, *Chemical Engineering Science*. 56 (2001) 4715-4724.
- [10] S. Hashemi, A. Macchi, P. Servio, *Chemical Engineering Science*. (submitted).
- [11] M.A. Trebble, P.R. Bishnoi, *Fluid Phase Equilibria*. 35 (1987) 1-18.
- [12] W.M. Deen, *Analysis of Transport Phenomena*, Oxford University Press, New York, 1998.
- [13] R.H. Perry, D.W. Green, *Perry's Chemical Engineer's Handbook*. 7th Edition ed, McGraw-Hill, 1997.
- [14] C.R. Wilke, P. Chang, *A.I.Ch.E. Journal*. 1 (1955) 264-270.
- [15] W. Hayduk, H. Laudie, *A.I.Ch.E. Journal*. 20 (1974) 611-615.
- [16] S.G. Kane, T.W. Evans, P.L.T. Brian, A.F. Sarofim, *A.I.Ch.E. Journal*. 20 (1974) 855-862.
- [17] A. Chapoy, A.H. Mohammadi, A. Chareton, B. Tohidi, D. Richon, *Ind. Eng. Chem. Res.* 43 (2004) 1794-1802.
- [18] J. Gaudette, P. Servio, *J. Chem. Eng. Data*. (submitted).

Captions for figures

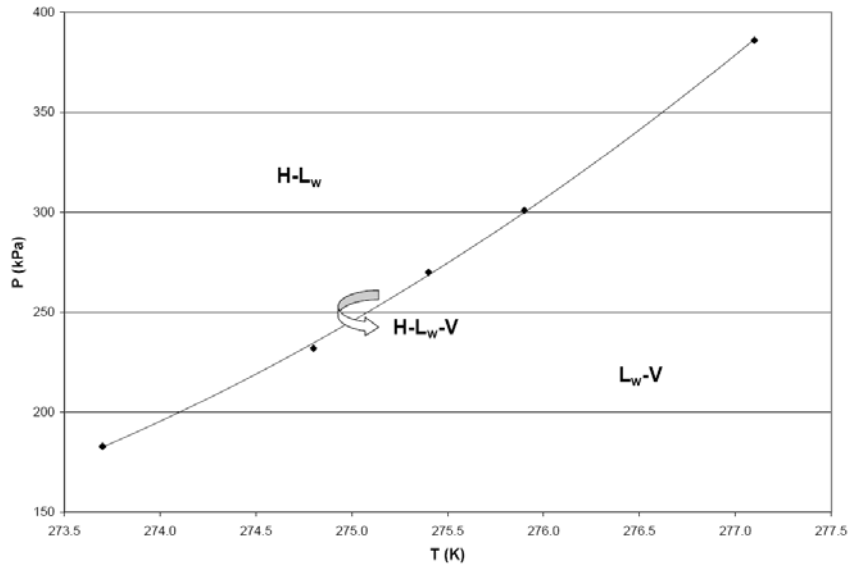


Figure 1: Propane-water phase diagram using the experimental data of Deaton and Frost [1]

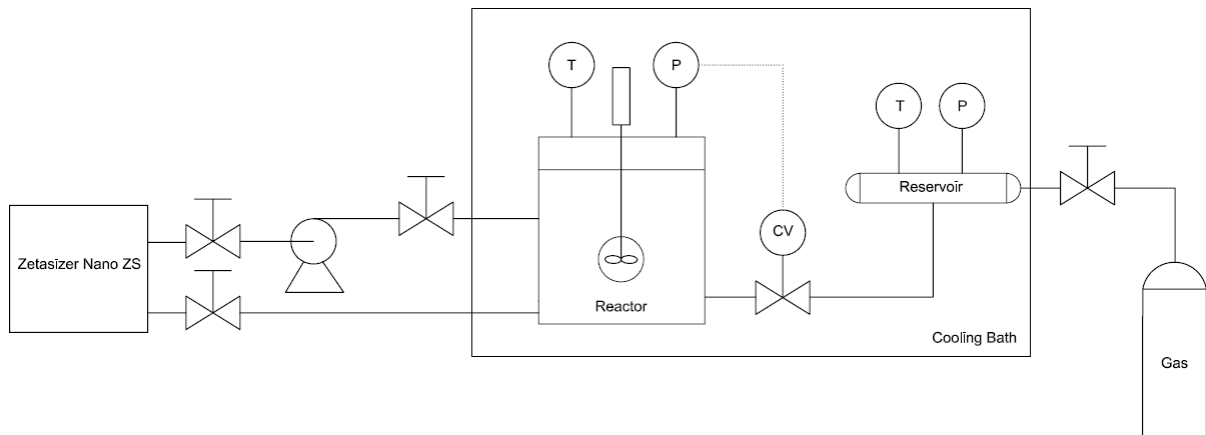


Figure 2: Simplified schematic of the experimental setup

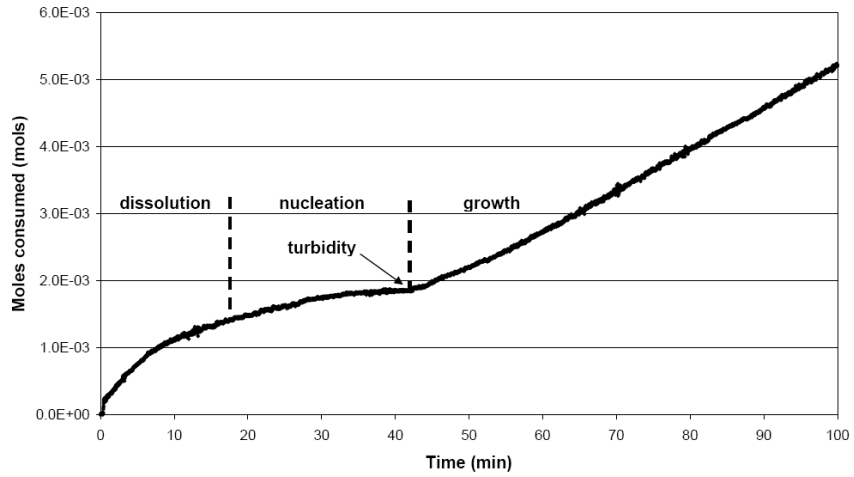


Figure 3: Mole consumption plot at 274.0 K and 212.4 kPa using propane

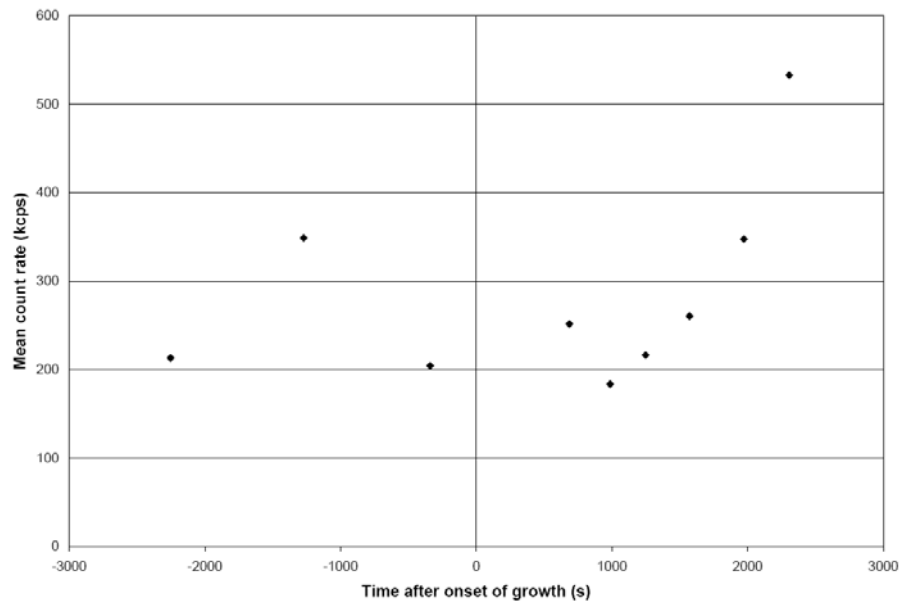


Figure 4: Mean count rate at 274.1 K and 214.8 kPa

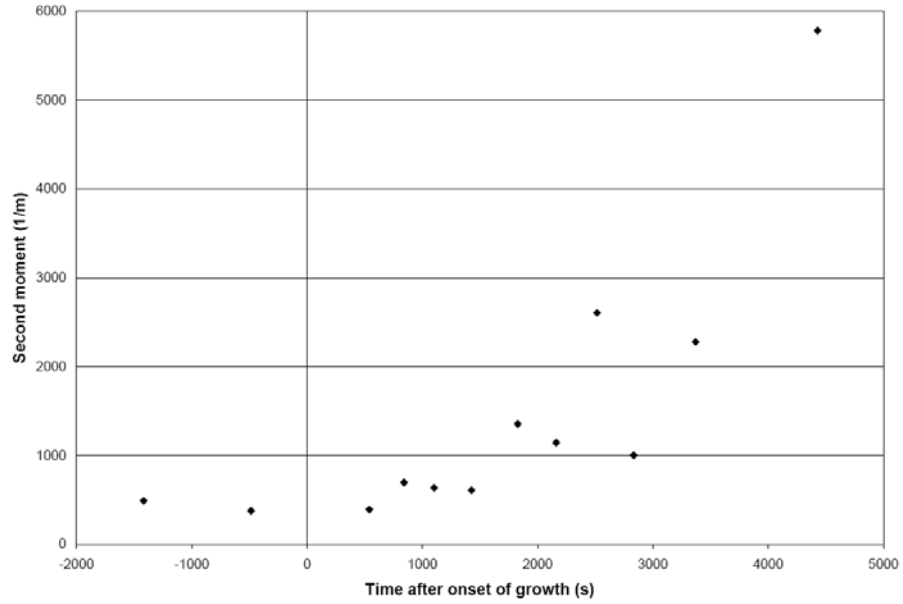


Figure 5: Second moment of the particle size distribution at 274.1 K and 214.8 kPa

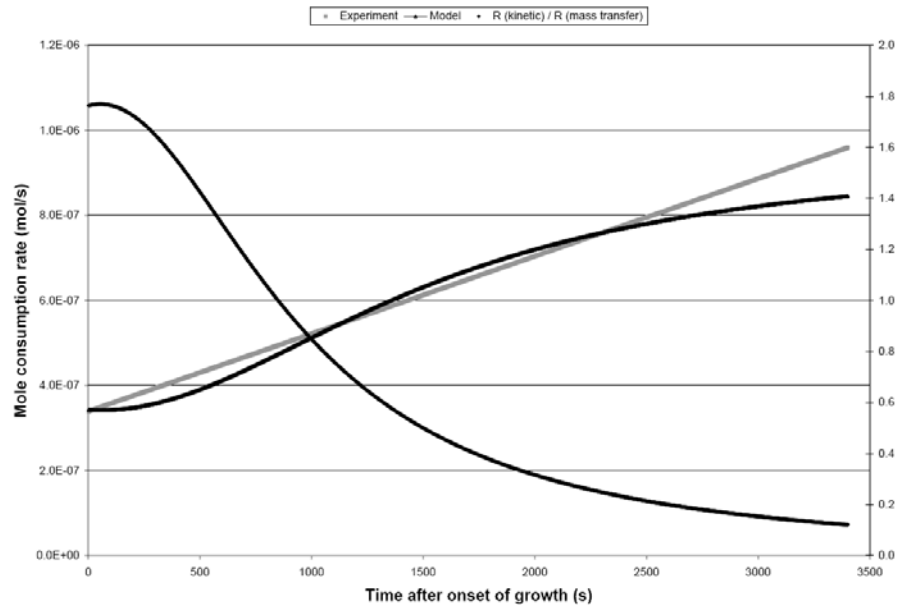


Figure 6: Kinetic model using the experimental reaction rate constant at 274.1 K and 214.8 kPa

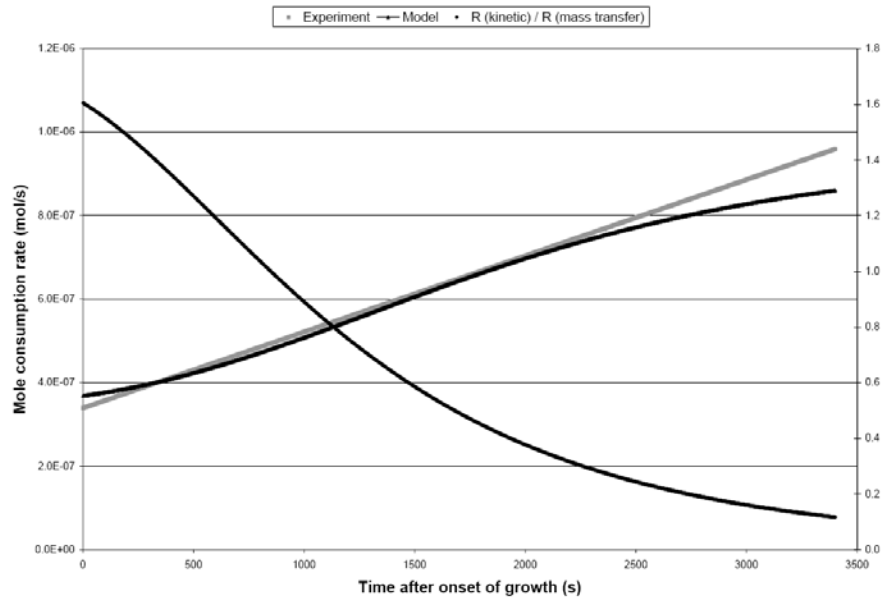


Figure 7: Kinetic model using the theoretical reaction rate constant at 274.1 K and 214.8 kPa